Materials Transactions, Vol. 48, No. 9 (2007) pp. 2319 to 2323
Special Issue on Solidification Science and Processing for Advanced Materials

Characterization and Mechanism of 304 Stainless Steel Vibration Welding

Che-Wei Kuo*, Chi-Ming Lin*, Gen-Huey Lai*, Yu-Che Chen*, Yung-Tse Chang* and Weite Wu

National Chung Hsing University, Institute of Materials Science and Engineering, 250 Kuo Kuang Road, Taichung 402, Taiwan, R. O. China

Gas tungsten arc welding (GTAW) was performed on AISI 304 stainless steel; steady-state vibration was produced by a mass-eccentric motor. The vibration weld shows a very small δ-ferrite structure, uniform composition distribution, less residual stress and less δ-ferrite content relative to the weld without vibration. The results illustrate that the vibration reduces the micro supercooling and improves the nucleation of δ-ferrite to form a grain refined structure. Vibration-induced stacking faults are identified as the major cause of the line broadening of X-ray diffraction profile. Correlating the literature and the result in the study, the mechanism of vibratory stress relief can be represented as the breakdown of dislocation into a pair of partial dislocations. This mechanism can comprehensively explain all the phenomena that take place during vibratory stress relief. [doi:10.2320/matertrans.MB200706]

(Received February 9, 2007; Accepted April 16, 2007; Published August 25, 2007)

Keywords: *vibration welding, δ-ferrite, X-ray diffraction, residual stress, grain refining*

1. Introduction

The microstructure of steel is largely modified and positively influenced by heat treatment, resulting in recrystallization, homogenization of segregation and elimination of harmful precipitates. However, in welding, such possibilities are rather limited, since welded components can, in rare instances, be affected by heat and be solution annealed or quenched and tempered. Therefore, the structure of welded metal is considerably less favourable and less homogeneous than that of the base metal.

A few years ago, vibration was used for improving the quality of metal which solidified from the melt, especially to improve the microstructures, mechanical properties and relieve the residual stress.[1–5] Over the past years, the use of vibration for stress relief or to enhance the properties of solidifying metal has become wide-spread throughout industry, despite the lack of scientific data regarding the phenomenon.

Important information about the theory of VSR (vibratory stress relief) should be mentioned. R. Dawson and D. G. Moffat indicate that vibrations are essential for stress relief because they induce micro strain in high-stress regions.[6] That is, the strain can be reduced by lattice slip. Then, a simple theory of bulk plastic flow due to the combination of the residual stress with the applied stress is often cited;[7] hereafter, this is referred to as the 'standard model'. The standard model postulates that the stress is relieved when the combination of the residual stress and the vibrating stress exceeds the yield strength of the material; the assumption is that the subsequent plastic flow is such that when the vibrational amplitude is removed, the previously stressed area can now return to a low level of residual stress. This is because the plastic deformation processes in metals are indicative of a process of dislocation movement. It has been postulated that the dislocation segments, released from weakly pinning point defects by cyclic loading, migrate towards a more stable configuration under the influence of internal stresses and thermally excited lattice vibrations. C. A. Walker, A. J. Waddell and D. J. Johnston found that dislocation multiplication occurred as the vibratory cycle increased and the multiplication stopped at the end of the VSR.[8] This illustrated that the strain reduced as the dislocation increased. These phenomena imply that the strain energy was released by dislocation proliferation during vibration.

AISI 304 stainless steel was used in this research. In austenitic steel welding, the transformation process is more complicated, and involves the transformation of δ into γ. Austenitic steel is composed of iron, chromium and nickel. This composition is close to the three-phase sector ($L + \gamma + \delta$). In 304 stainless steel, the existence of only one γ-austenite is normal; however, the weld always contains residual δ-ferrite of approximately 5–10%. The δ-ferrite results from microsegregation during solidification, followed by solid-state transformation controlled by the diffusion during subsequent cooling.[9] The δ-γ transformation normally occurs quickly during welding, producing dendrite growth and segregation. It is difficult to discriminate between the δ and γ compositions of the weld. This problem was studied by Lichtenegger and Blöch;[10] it was found that the Cr and Ni contents in the residual δ-ferrite were higher in a metal alloy weld than those in the original specimen. Therefore, observing the residual δ-ferrite is useful for understanding the difference between the solidifying processes in vibration welding and non-vibration welding.

2. Experimental Procedures

2.1 Welding process

As-received AISI 304 austenitic stainless steel plate was used. The plate was 70 mm × 25 mm × 3 mm. Specimens were welded using the gas tungsten arc welding (GTAW) process without a filler metal. The welding current was 60 A; the voltage, 9 V; and the traveling speed, 96 mm/min. A tungsten rod of 2.4 mm diameter, protective argon gas (15 IPM) and an acetone-cleaned pre-weld were used. Before determining the vibration frequency for welding, the welding

*Graduate Student, National Chung Hsing University

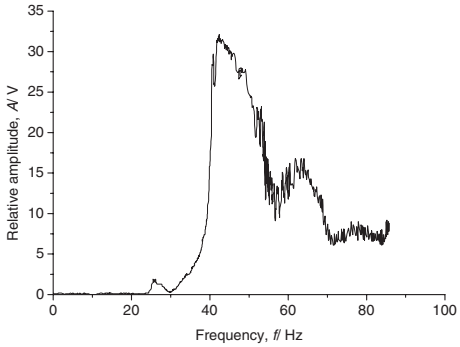

Fig. 1 Harmonic curve of the welding system.

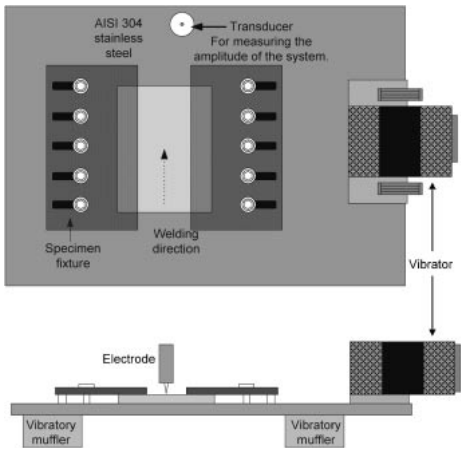

Fig. 2 Synchronized vibration welding system.

table was continuously vibrated for 20 min until the system reached the steady-state. Then, the data for the harmonic curve of the vibration welding system was obtained by using a transducer with a vibration controller and a data (frequency and amplitude) recorder; this curve is shown in Fig. 1. Figure 2 shows the synchronized vibration welding system. The vibration welding was performed at a sub-resonant frequency.[2)] The sub-resonant frequency was defined as the frequency which had one-third the resonant amplitude or which was 10 Hz less than the resonant frequency. Sub-resonant frequency was thought to input more energy to the object than the resonant frequency. The sub-resonant frequency was 39.4 Hz (with one-third the resonant amplitude). The resonant frequency of the welding system was 43.3 Hz. The specimens were welded under two conditions: subjected to vibrations of 0 Hz and 39.4 Hz.

2.2 Microscopy, chemical composition, and δ-ferrite content measurement

The microstructures of the welded specimens were investigated using optical microscopy. Conventional etching compounds react particularly with the secondary structures. If these compounds are employed, the primary structure is only hardly, or not at all, visible. Revealing the primary structure requires the use of the so-called primary etchants that react with the segregations of the primary solidified structure. The LB 1 colour etchant (Lichtenegger and Blöch etch) was used, which makes both primary and secondary

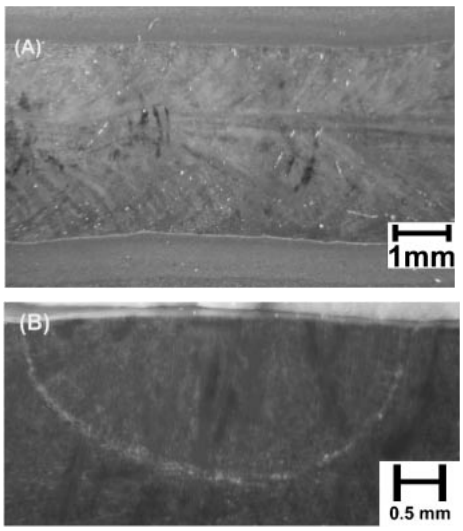

Fig. 3 Weld bead of welding without vibration. (A) Top view (B) Cross section.

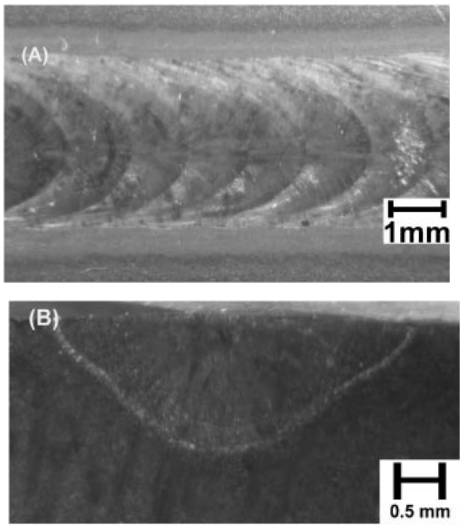

Fig. 4 Weld bead of vibration welding. (A) Top view (B) Cross section.

structures visible.[10)] Etching was performed using 0.5 g of $K_2S_2O_5$ and 20 g of $NH_4F{\cdot}HF$ in 100 mL H_2O at 70–80 °C until the sample became tinted. Colour etching was set up in such a way as to illustrate the situation during the solidification of the weld metal when about three-fourths of the weld-metal volume has solidified and one-fourth is still present as liquid residual melt. In Fig. 5, the blue area of the structure represents the already solidified cellular structure, which consists of primary δ-ferrite. A bright structural constituent is also visible in the primary precipitated cellular δ-ferrite. This represents the portion of the residual δ-ferrite that remains after δ-γ transformation from the primary precipitated δ-ferrite at ambient temperature. The residual melt exists between all the blue structures, which appears as a brownish-tinted structural constituent. The chemical compositions of residual δ-ferrite (white), primary precipitate δ-ferrite (blue) and residual melt (orange) in Figs. 5 and 6 were identified by field emission scanning electron microscope (FESEM, JEOL JSM 7000F) equipped with energy disper-

sive spectrometer (EDS). The δ-ferrite content was measured by a magnetic scope (Fischer Feritscope MP30).

2.3 X-ray diffraction stress measurement

The measurements were performed with a MAC SCIENCE MXP3 (40 kV, 30 mA, CuK_α radiation, $K_\alpha = 1.54056$ nm. The γ-Fe reflection under study was {331}, which produces a Bragg peak at $2\theta = 148.4^\circ$ for the aforementioned wavelength. Within each cross-section, two generatrices were sampled, located at 0° and 45°.

The application of X-ray-diffraction (XRD) stress measurements to practical engineering problems began in the early 1950s. As in all diffraction methods, the lattice spacing is calculated from the diffraction angle, 2θ, and the known X-ray wavelength using Bragg's law. The precision necessary for strain measurement in engineering materials can be achieved using the diffraction peaks produced in the high back-reflection region in which $2\theta > 120^\circ$. The macrostrain is determined from shifts, typically $<1^\circ$, of the mean diffraction-peak position. Residual stress can be expressed as follows. Details of this equation are given elsewhere[11] (Young's modulus: 193, 100 MPa; Poisson's ratio: 0.29).

$$\sigma_\psi = \left(\frac{\mathrm{E}}{1+\nu}\right)_{(\mathrm{hkl})} \frac{1}{\mathrm{d}_0} \left(\frac{\partial d_{\phi\psi}}{\partial \sin^2 \Psi}\right)$$

σ_ψ: Residual stress
ν: Poisson's ratio
E: Young's modulus
d_0: Stress-free lattice spacing

3. Experimental Results and Discussion

The morphologies of weld bead without and with vibration are shown in Figs. 3 and 4, respectively. The top view of vibrationless welding shows a flatness surface, different from the wavy surface of vibration welding. As to the shape of cross section, the outline of vibration welding displayed a salient at the bottom of welding pool (Fig. 4B) which implies that vibration offered an to force burst the bottom of weld pool. The perturbation causes liquid convection of vibration welding different from without vibration welding, and the phenomenon will affect the solidification parameter and further more on the microstructure and ferrite percent.

Figure 5 shows the solidification structure of 304 stainless steel weld metal, which has solidified to form primary δ-ferrite. In this area, the δ-ferrite dendrite was a heterogeneous nucleation that formed from the liquid melt. Dendrite growth and the resulting dendrite structure are related to the undesirable effects in interdendritic liquid, with its inhomogeneous concentrations. The primary precipitate, δ-ferrite, also emerges as the second dendrite arm from the major arm because of the huge constitutional supercooling. This phenomenon has been described elsewhere.[12] The microstructure of the weld bead for vibration welding is shown in Fig. 4. The dendrite arm of δ-ferrite is much shorter, only 4–5 µm in length, than that in the case of the vibrationless welding in which it is a big, thick structure, approximately 10–12 µm in length. The difference in dendrite size shows that the constitutional supercooling of liquid metal significantly decreased under vibration. On the other hand, the amount of nuclei increased. For welding without vibration, the amount of nuclei was approximately 1.04 per 100 μm^2; this value increased to 3.65 per 100 μm^2 for vibration welding. This increase in the amount of nuclei limited the growth of the δ-ferrite dendrite arm which consequently formed a very fine structure. The increase in the rate of nucleation resulted from the vibration-induced convection in the weld pool, which caused partially melted grains to detach from the solid–liquid mixture surrounding the weld pool. Like dendrite fragments, these partially melted grains, if they survive in the weld pool, can act as nuclei for the formation of new grains in the weld metal.[4]

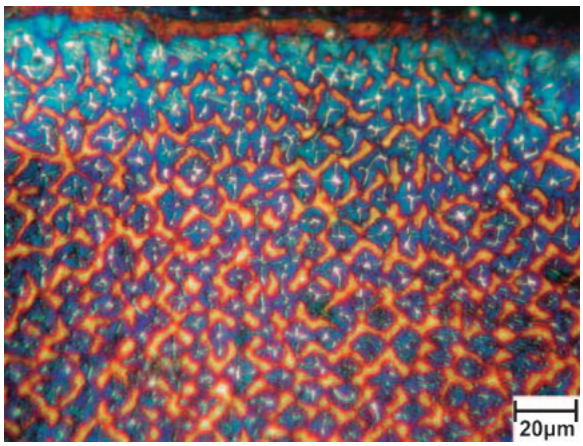

Fig. 5 Top of the weld bead (welding without vibration).

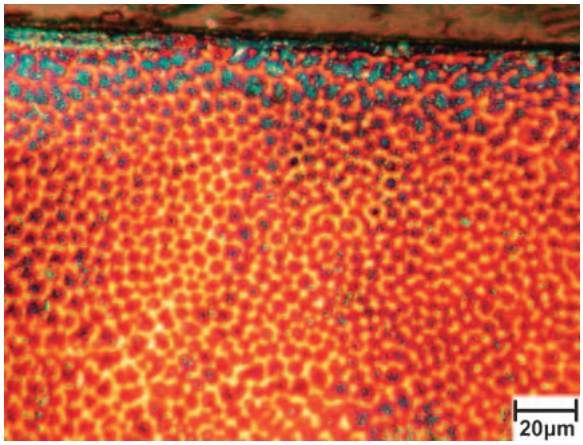

Fig. 6 Top of the weld bead (welding with vibration).

Another important distinction between general (without vibration) and vibration welding is the composition uniformity. In this case, colour etched optical micrographs can clearly display the divergence of chemical concentration. Colour etching is a controlled corrosion process based on an electrolytic action between the surface areas at different potentials. In the etching of AISI 304 stainless steel, a potential difference exists between the γ and δ phases and concentration gradients in the γ phase. Figure 6 shows a more uniform composition distribution than that in Figure 5. The blue (primary precipitate δ-ferrite) area embracing bright tiny part (residual δ-ferrite) is smaller in Fig. 6 than in Fig. 5. The chemical compositions of the residual, primary precip-

Table 1 Chemical compositions by EDS. δ_r: residual δ-ferrite, δ_p: primary precipitate δ-ferrite, R_m: residual melt.

Weight%	Without vibration			With vibration		
	δ_r	δ_p	R_m	δ_r	δ_p	R_m
Cr	19.14	18.87	18.27	19.66	19.25	18.50
Fe	69.01	67.61	68.91	67.65	67.89	69.53
Ni	11.85	13.52	12.81	12.70	12.86	11.96

Table 2 Results of δ-ferrite content measurement. Values are given in %.

Frequency											Average
0 Hz	4.3	3.2	3.3	3.7	5.5	4.6	5.5	5.0	4.5	5.2	4.48
39.4 Hz	3.1	2.7	2.5	2.4	3.0	1.5	1.1	2.0	1.8	1.8	2.19

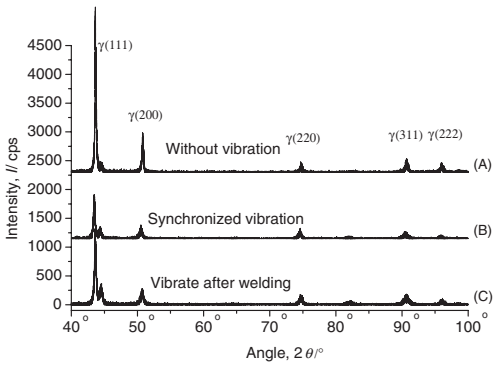

Fig. 7 XRD pattern for 304 stainless steel. (A) Without vibration. (B) With vibration. (C) Vibrate after welding.

Table 3 FWHM of the XRD planes. (A) Without vibration. (B) With vibration. (C) Vibrate after welding.

Plane index	FWHM,		
	A	B	C
(111)	0.203°	0.269°	0.275°
(200)	0.258°	0.490°	0.461°
(220)	0.343°	0.463°	0.491°
(311)	0.378°	0.745°	0.778°
(222)	0.279°	0.599°	0.599°

itate δ-ferrite and residual melt are listed in Table 1. The same composition tendency is observed for both the cases of welding, namely, without vibration and with vibration. The Cr content is the highest for the residual δ-ferrite, followed by the primary precipitate δ-ferrite; the residual melt has the lowest Cr content. This result implies that the difference in divergence of chemical concentration was limited to a small zone. The difference could be attributed to the small constitutional supercooling and fine grain structure such that the local chemical concentrations were more finely and smoothly distributed. This can avoid the serious segregations caused by the solidifying process in the weld.

The δ-ferrite content was measured using a ferritescope, and the results are listed in Table 2. The average δ-ferrite content for the non-vibration and vibration welding is 4.48% and 2.19%, respectively. As shown in Table 1, δ-ferrite has a higher Cr content than γ-austenite, and less δ-ferrite implies less segregation. These δ-ferrite contents indicate that vibrations decrease the temperature gradient of melt pool and enable the liquid metal to solidify to form a uniform structure with less segregation.

The residual stresses in the non-vibration and vibration welding are 262 MPa and 206 MPa, respectively. In the vibration welding, the residual stress is smaller by 56 MPa; this implies that approximately one-fifth of the residual stress can be reduced by vibration. Vibration applied during welding needs less time for residual stress relief. In this study, a residual stress test was performed on samples cut from the center of the weld bead; it melted and solidified under vibration applied only for 15–20 s. The vibration and the welding stopped simultaneously. As compared to vibration welding, vibration after welding takes more time and energy because the yield point at room temperature is greater than that at a higher temperature.

Figure 7 shows the XRD profiles; A and B show the weld formed without and with vibration, respectively. In order to discriminate the effect of vibration but not the nucleation process, a test was performed in which the specimen was vibrated for 20 min; the results are shown in Figure 7(C). The intensity shown in Fig. 7(A) is the highest intensity, followed by that in (C); and (B) has the lowest. Their FWHM (full width at half maximum) were determined by curve fitting using a Gaussian function. The most obvious distinctions between the three conditions are the peak intensity and the width, especially when the vibration was applied. The diffraction line broadening,[13] is caused by three major factors: nonuniform strain, small particles and stacking fault.

Nonuniform strain was induced by manufacturing into local area and causes the lattice constant to deviate from a uniform value. This leads the diffraction line to distribute in a range of 2θ values, resulting in line broadening (Table 3). In the study, three samples have the same stress distribution because they were fabricated using the same welding process. Hence, nonuniform strain cannot be the cause of line broadening. Further, the grain size must be smaller than 0.1 μm in order to cause line broadening. Thus, the stacking fault can be identified as the major cause of diffraction line broadening.

The significant implications of the VSR mentioned above are as follows:

(1) Plastic deformation is necessary for stress relief and is correlated with the amplitude of vibration but not the frequency.[6] (2) Dislocation multiplication takes place during stress relieving; when the stress relief ends, the dislocation multiplication stops, too.[8] An increase in the dislocation density during plastic manufacturing is very usual. The distinction between VSR and plastic manufacturing is that the vibration can induce only a very small force. According the standard model,[7] the force needed for plastic deformation is contributed by the residual stress and the vibrating stress, and their sum must exceed the yield strength. For this reason, the vibration has no effect on the area with a low residual stress and the effect of vibration can be ignored.

To integrate the phenomenon of VSR from that in the pervious study and this study, dislocation movement, dislocation multiplication and increase of stacking fault

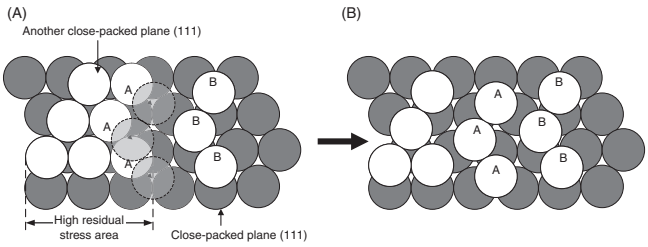

Fig. 8 Stress relief during vibration welding.

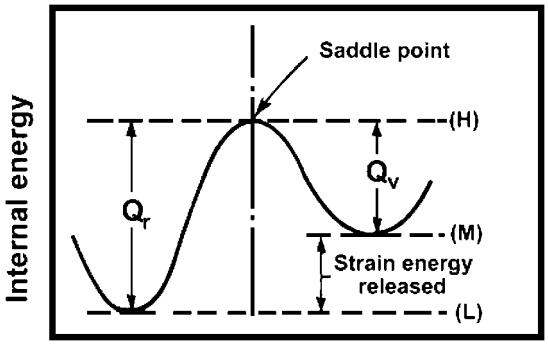

Fig. 9 Energy states of atoms in the VSR process.

density are considered. The reasonable processes that took place during the VSR can be outlined. First, we consider the plastic deformation. Its mechanism in an fcc crystal has been illustrated.[14] During VSR, the dislocation shown in Figure 8 tends to move towards the left. Atoms A with a high residual stress are on the meta-stable sites. Atoms A cannot slip to the low-energy sites unless they obtain an extra energy to overcome the barrier. When vibration is applied, atoms A have sufficient energy to slip and fit into the dotted circles shown in Fig. 8; then, the strain is released. The process involves the breakdown of the total dislocation into two partial dislocations and can be expressed according to the relation of Burgers vector.[14]

$$\frac{1}{2}[\bar{1}10] = \frac{1}{6}[\bar{1}2\bar{1}] + \frac{1}{6}[\bar{2}11]$$

Another mechanism, 'extended dislocation',[14] induce the rearrangement of the atoms; consequently, the strain would be released. If dislocation density stops increasing, the VSR is terminated. After the dislocations break down, the dislocation density and the number of stacking faults increase because the two sides of the dislocation constitute new stacking faults. These phenomena corresponded with the literature referred and were observed in the study. It can also be well expressed by the energy state diagram.

The atoms with high residual stress are meta-stable, and their energy state is at (M), as shown in Fig. 9. If the vibration provides energy Q_v, then the meta-stable atoms with internal energies higher than (M) can cross over the saddle point (H) and release their internal energies Q_r to a stable state (L). If the vibration energy is higher than Q_v, then the atoms with low residual stress can cross slip and fit into the low-energy sites and release the strain energy. This is why VSR has no relation with vibration frequency; the higher the amplitude, the more is the stress relief.

4. Conclusions

In this study, we investigated the effect of vibration welding on the microstructure, δ-ferrite content, residual stress and XRD profile of 304 stainless steel. The mechanism of VSR was discussed. The following results were obtained.

(1) Vibration affects the welding pool shape and the convection of welding pool strongly. It will affect the solidifying parameter and metallurgic properties.
(2) Dendrite arm of the δ-ferrite became very short and fine under vibration welding because the constitutional supercooling was decreased by vibration.
(3) Vibration improves the nucleation of δ-ferrite, which precipitates from the liquid phase. The large amount of δ-ferrite blocks its growth, resulting in the formation of a fine and uniform structure with low δ-ferrite content.
(4) The residual stress reduced from 262 to 206 MPa when vibration was applied during welding even if the vibration time was only 15~20 s.
(5) XRD line broadening of the vibration weld revealed that the vibration welding induces stacking faults. According to pervious studies, the dislocation movement followed by dislocation breakdown is identified as the major cause of stress relief.

Acknowledgement

This work was partially supported by the National Science Council, Taiwan, R.O.C., under project NSC 92-2216-E-005-005.

REFERENCES

1) G. Gnirss: Indian Weld. J. **22** (1990) 11–16.
2) Jr. G. Hebel August: Metal Prog. **128** (1985) 51–55.
3) W. Wu, D. Y. Lin and S. H. Chen: J. Mater. Sci. Lett. **18** (1999) 1829–1831.
4) B. Wei: Acta Mater. **40** (1992) 2739–2751.
5) W. Wu: Scr. Mater. **42** (2000) 661–665.
6) R. Dawson and D. G. Moffat: J. Eng. Mater. Technol.-Trans. ASME. **102** (1980) 169–176.
7) E. Klotzbucher and H. Kraft: *Residual Stresses in Science and Technology*, (DGM Metallurgy Information, USA, 1987) p. 959.
8) C. A. Walker, A. J. Waddell and D. J. Johnston: *Proc. Instn. Mech. Engrs.* **209** (1995) 51–58.
9) P. Bilmes, A. Gonzalez, C. Llorente and M. Solari: Welding Int. **10** (1997) 18–29.
10) E. Folkhard: *Welding Metallurgy of Stainless Steels*, (Springer-Verlag, Wien, 1984) pp. 63–70.
11) M. E. Hilley, J. A. Larson, C. F. Jatczak and R. E. Richlefs, editors. *Residual Stress Measurement by X-ray Diffraction*, SAE Information Report J784a (1971) pp. 19–24.
12) Sindo Kou: *Welding Metallurgy*, 2nd ed., (John Wiley & Sons, New York, 2003) pp. 181–188.
13) B. D. Cullity: *Elements of X-Ray Diffraction*, 2nd ed., (Addison Wesley, London, 1978) pp. 285–292.
14) Robert E. Reed-Hill: *Physical Metallurgy Principles*, 3rd ed., (PWS., Boston, 1994) pp. 103–107.